Research Article

Journal of PeptideScience

Received: 20 August 2010 Revised: 23 March 2011 Accepted: 20 April 2011 Published online in Wiley Online Library: 10 June 2011

(wileyonlinelibrary.com) DOI 10.1002/psc.1384

Structural scaffold for eIF4E binding selectivity of 4E-BP isoforms: crystal structure of eIF4E binding region of 4E-BP2 and its comparison with that of 4E-BP1

Ai Fukuyo, Yasuko In, Toshimasa Ishida and Koji Tomoo*

To clarify the higher eukaryotic initiation factor 4E (eIF4E) binding selectivity of 4E-binding protein 2 (4E-BP2) than of 4E-BP1, as determined by Trp fluorescence analysis, the crystal structure of the eIF4E binding region of 4E-BP2 in complex with m^7GTP-bound human eIF4E has been determined by X-ray diffraction analysis and compared with that of 4E-BP1. The crystal structure revealed that the Pro47-Ser65 moiety of 4E-BP2 adopts a L-shaped conformation involving extended and α-helical structures and extends over the N-terminal loop and two different helix regions of eIF4E through hydrogen bonds, and electrostatic and hydrophobic interactions; these features were similarly observed for 4E-BP1. Although the pattern of the overall interaction of 4E-BP2 with eIF4E was similar to that of 4E-BP1, a notable difference was observed for the 60–63 sequence in relation to the conformation and binding selectivity of the 4E-BP isoform, i.e. Met-Glu-Cys-Arg for 4E-BP1 and Leu-Asp-Arg-Arg for 4E-BP2. In this paper, we report that the structural scaffold of the eIF4E binding preference for 4E-BP2 over 4E-BP1 is based on the stacking of the Arg63 planar side chain on the Trp73 indole ring of eIF4E and the construction of a compact hydrophobic space around the Trp73 indole ring by the Leu59-Leu60 sequence of 4E-BP2. Copyright © 2011 European Peptide Society and John Wiley & Sons, Ltd.

Keywords: 4E-BP1; 4E-BP2; eIF4E; ternary complex; X-ray crystal structure; binding preference

Introduction

Eukaryotic translation initiation is performed by many eukaryotic initiation factors (eIFs) and regulated through structural changes in the phosphorylation states of eIFs and endogenous regulator proteins [1]. In the cap-dependent translation of mRNA, an interaction is required between the cap structure and the eukaryotic initiation factor 4F, a supramolecular complex of three subunits, eIF4E, eIF4A and eIF4G, for the efficient translation of mRNA. The first step in the translation process is the binding of eIF4E, the smallest subunit in eIF4F, to the mRNA cap structure. Because this is the rate-limiting step in translation initiation, eIF4E serves as a master switch that controls eukaryotic translation and a pivot molecule for translational control [2]. As the initiation function of eIF4E is controlled by the association/dissociation with the endogenous 4E-binding protein (4E-BP) [1,3,4], the study on the interaction of eIF4E with 4E-BP is therefore important in understanding the regulation mechanism of such a process.

At present, three isoforms of 4E-BP, namely, 4E-BP1–4E-BP3, are known [1,3] and their sequences are shown in Figure 1. Concerning the function of the 4E-BP, it is known that (i) these isoforms bind to eIF4E through a sequence of the $Y(X)_4L\phi$ motif (X: variable, ϕ: hydrophobic, see Figure 1) [5,6], (ii) the hyperphosphorylations of their Thr and Ser residues in response to growth factors and mitogens result in their release from eIF4E [4,7], and (iii) although 4E-BP1 and 4E-BP2 themselves show a random structure, their eIF4E binding regions form a helical structure upon binding to a conserved surface on the dorsal side of the eIF4E cap-binding pocket [3,4]. In contrast, the functional difference of these isoforms upon binding to eIF4E is poorly understood. For more insight, we previously measured the interactions of these 4E-BP isoforms with eIF4E by the Trp fluorescence titration method [8] and observed the binding preference of eIF4E for 4E-BP2 over 4E-BP1 and 4E-BP3 under a physiological condition, where the association constant of 4E-BP2 was two- to threefold larger than that of 4E-BP1. However, it became clear by surface plasmon resonance measurement that the association constants of eIF4E with 4E-BP1–3 isoforms are almost within the same range (unpublished data). This disagreement indicates obviously that the local interaction mode at the binding site is meaningfully different, although the overall interaction model of eIF4E with 4E-BP is nearly same. Thus, it is reasonable to consider that the binding preference shown by the Trp fluorescence titration results from the difference between 4E-BP1 and 4E-BP2 in the mode of interaction of the Trp73 residue of eIF4E, especially the 4E-BP1-specific Met-Glu-Cys and 4E-BP2-specific Lys-Asp-Arg (60–62) sequences, because the direct participation of the Trp73 residue of eIF4E in the binding with 4E-BP isoform is shown by the X-ray crystal structure of the eIF4E–4E-BP1 fragment complex [9].

Previously, we reported the crystal structure of the ternary complex of m^7GpppA–eIF4E–4E-BP1 fragment (Thr36-Thr70) [8]. Therefore, to clarify the difference in the microscopic situation at

* *Correspondence to: Koji Tomoo, Laboratory of Physical Chemistry, Osaka University of Pharmaceutical Sciences, 4-20-1 Nasahara, Takatsuki, Osaka 569-1094, Japan. E-mail: tomoo@gly.oups.ac.jp*

Laboratory of Physical Chemistry, Osaka University of Pharmaceutical Sciences, 4-20-1 Nasahara, Takatsuki, Osaka 569-1094, Japan

Journal of PeptideScience

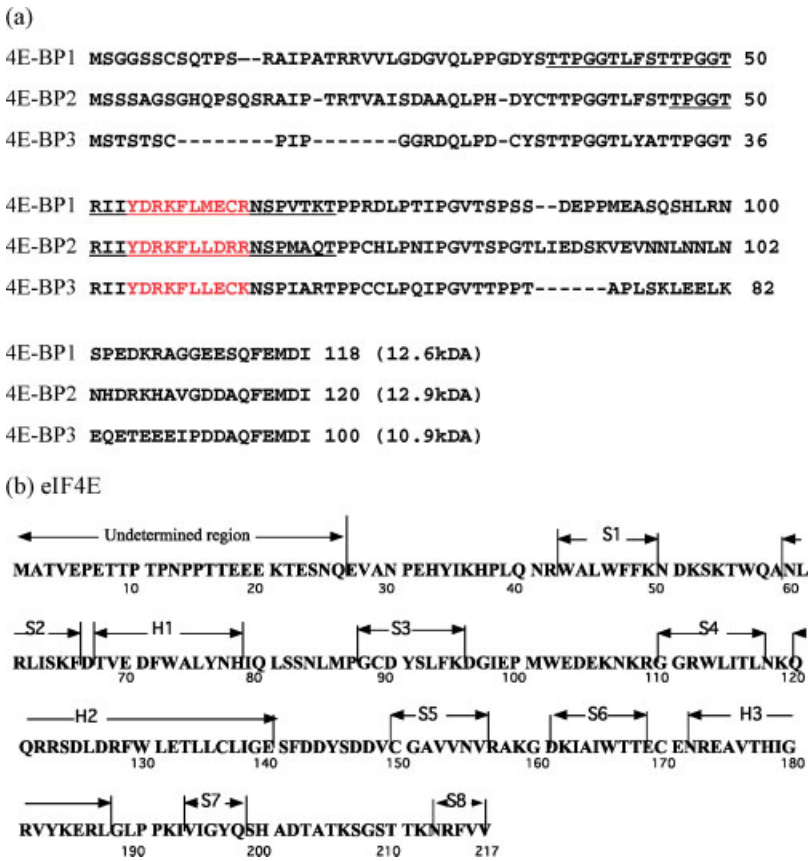

Figure 1. Amino acid sequences of (a) 4E-BP1–3 isoforms and (b) eIF4E. The sequences of (a) are aligned on the basis of their functional similarities. The eIF4E α-helical binding region of the 4E-BP isoforms is shown in bold. The sequences of the 4E-BP1 and 4E-BP2 peptides used for the complex formation are underlined. The secondary structural elements of eIF4E (b) elucidated by X-ray crystal analysis are indicated by H1–H3 and S1–S8, which correspond to the helices and strand structures in Figure 3, respectively.

eIF4E binding site between 4E-BP1 and 4E-BP2 at the atomic level, we determined the crystal structure of the complex of m^{7}GTP-bound eIF4E with the 4E-BP2 fragment peptide (Thr46-Thr70), in which m^{7}GTP was used as a model of the mRNA cap structure, and compared with the X-ray result of the m^{7}GpppA–eIF4E–4E-BP1 peptide ternary complex. In this paper, we report these results and the structural scaffold for the eIF4E binding preference for 4E-BP2 over 4E-BP1.

Materials and Methods

Peptide Synthesis

The commercially available materials used were of reagent grade or higher purity. The Thr46-Thr70 fragment of 4E-BP2 used for the crystallization was synthesized using a solid-phase peptide synthesizer. The peptide (including TFA as the counter ion) was obtained in the form of lyophilized powder. The peptide was characterized by mass spectrometry and had a purity >95.0%, as determined by RP HPLC.

Preparation of Full-Length Human eIF4E

The commercially available reagents used for preparing recombinant proteins were purchased from either Sigma Chemical, Takara Shuzo, New England Biolabs Inc., Toyobo Co., Novagen Co., or GE Healthcare Co. The gene expression of human full-length eIF4E in *Escherichia coli* and the isolation and purification of the expressed protein were carried out according to a previous method [10]. The supernatant containing recombinant eIF4E was applied to an m^{7}GTP-Sepharose 4B affinity column equilibrated with buffer A (50 mM HEPES-NaOH (pH 7.5), 1 mM EDTA, 100 mM NaCl). The m^{7}GTP-bound eIF4E was prepared by elution with buffer B (buffer A + 100 μM m^{7}GTP). The solution was concentrated with Centricon 10 (Amicon Co.) to the desired concentration. The m^{7}GTP-bound eIF4E in buffer A was then incubated with an equimolar amount of the 4E-BP2 peptide and concentrated to a protein concentration of 5 mg/ml. Droplets of 2 μl initial volume were equilibrated at 18 °C against the reservoir solution (2 μl) of 100 mM MES (2-(*N*-morpholino)ethanesulfonic acid) buffer (pH 5.6) containing 0.2 M ammonium sulfate and 15–25% PEG-MME (monomethyl ether) 2000 (Hampton Res.).

X-ray Crystal Analysis

Needle-shaped crystals of the m^{7}GTP-eIF4E–4E-BP2 peptide ternary complex were obtained after 1 week by the hanging drop vapor diffusion method at 15 °C, growing up to dimensions of 0.05 mm × 0.05 mm × 0.5 mm. X-ray diffraction data at 100 K were collected using CuKα radiation from an FR-E rotating anode X-ray generator (Rigaku Corp) equipped with a confocal mirror (Osmic Inc.) and an R-AXIS VII detector. The crystal was cryoprotected using the cryosolvent prepared by adding 15–20% glycerol to the reservoir solution. Data processing was performed with the

Table 1. Crystallographic data and refinement statistics

Crystallographic data	
Cell dimensions (Å)	$a = b = 87.84, c = 37.75$
Space group	$P4_3$
Z	4
V_m (Å^3/Da)	3.08
Temperature (K)	100
X-ray source (Å)	1.54
Resolution (Å)	44–2.1
Unique reflection	16 431
Completeness (%)	95.4
R_{merge} (%)	10.1
Refinement statistics	
Resolution (Å)	30–2.2
Reflection	14 502
R-factor (%)	22.8
R_{free} (%)[3]	26.5
Number of atoms	
Protein	1735
m^{7}GTP	51
Water	94
Overall B protein (Å^2)	36
Estimated maximum coordinate error (Å)	0.26
RMS deviation	
Bond (Å)	0.007
Angle (°)	1.30
Improper	0.66

program CrystalClear [11]. The crystal diffracted up to a 2.1 Å resolution and the data were processed in a tetragonal lattice system.

The space group and cell constants were essentially the same as those of the m^{7}GpppA–eIF4E–4E-BP1 peptide ternary complex [8]. Thus, the initial structure of the present crystal was determined with the CNS program [12] using the atomic coordinates of the eIF4E (PDB code 1WKW). An atomic model of the complex was constructed using the TURBO-FRODO graphics program [13], and the structure was refined using the CNS program package. After several cycles of refinement, the difference electron density maps gave densities sufficient for constructing the entire m^{7}GTP structure and the Pro47-Ser65 moiety of the 4E-BP2 peptide, although the terminal sides of the peptide showed low densities due to the high temperature factors. Further refinement of the complex structure and the addition of clearly identifiable water molecules improved the *R*-factor. Data collection and refinement statistics are presented in Table 1. The final atomic coordinates have been deposited in the RCSB Brookhaven Protein Data Bank (the accession code is 3AM7).

Results and Discussion

Overall Structure of Ternary Complex

An overview of the ternary complex of m^{7}GTP-eIF4E–4E-BP2 peptide is shown in Figure 2, together with the electron density map of 4E-BP2 peptide moiety; the amino acid sequence and secondary structural elements of eIF4E are shown in Figure 1. The electron density from the N-terminal to Gln26 of eIF4E was not assigned because of the high thermal motion, and this structural flexibility in the N-terminal region was the same as that in the eIF4E–m^{7}GpppA binary complex [14] and the ternary complex with the 4E-BP1 fragment peptide [8]. Because the overall structure of eIF4E complexed with 4E-BP2 was essentially the same as that with 4E-BP1 complex (the rms deviation between their whole atomic coordinates was 0.08 Å), it could say that the interactions of eIF4E with 4E-BP1 and 4E-BP2 are essentially unaffected by the difference between m^{7}GpppA and m^{7}GTP used as a model of mRNA cap structure in the respective complexes. The entire structure of 4E-BP2 peptide (Thr46-Thr70) was not observed, and the electron density was detected for the Pro47-Ser65 moiety (Figure 2); this was the same as the 4E-BP1 peptide. The rms deviation between the whole atomic coordinates of 4E-BP2 and 4E-BP1 peptides was 2.48 Å.

The 4E-BP2 peptide was localized at the dorsal N-terminal root surface of the eIF4E cap-binding pocket and adopted a L-shaped open form, where the Asp55-Arg63 moiety formed an α-helical secondary structure and the Pro47-Tyr54 and Asn64-Ser65 sequences were in an extended conformation, without adopting any defined secondary structure; similar L-shaped conformation was observed for 4E-BP1peptide. As the CD spectra of full-length 4E-BP1 ~3 and their fragment peptides including the Y(X)$_4$Lϕ sequence show a random conformation in the isolated state, it is evident that the eIF4E binding region is induced to adopt an α-helical structure by interacting with eIF4E. The peptide is mainly fixed by hydrogen bonds, and electrostatic and hydrophobic interactions with three structural parts of eIF4E, i.e. the N-terminal loop (His37-Gln40), H1 helix (Val69-Asn77) and H2 helix (Glu132-Glu140) regions. The present result confirmed the importance of Tyr54, Leu59 and Leu60 in the Y(X)$_4$Lϕ sequence for the interaction with eIF4E (to be discussed later).

Conformations of 4E-BP Isoforms

The molecular conformation of 4E-BP2 is shown in Figure 3, together with that of 4E-BP1 for comparison. Possible intramolecular hydrogen bonds and selected electrostatic short contacts are given in Table 2. The conformation of 4E-BP2 is affected not only by the interaction at the eIF4E binding pocket, but also by the crystal packing, because the interatomic short contacts of 4E-BP2 are formed between the neighboring eIF4E in the crystal; similar affect was also observed for the conformation of 4E-BP1. The overall structures of both peptides are similar in such a way that the sequences of the N- and C-terminal sides adopt the extended (Pro47-Tyr54) and α-helical (Asp55-Arg63) conformations, respectively. However, notable differences are observed between the structurally rigid α-helical moieties. In addition to the difference in hydrogen bonding pattern between the 60 and 64 sequences of both peptides (Table 2), one remarkable feature of 4E-BP2 is the intramolecular $\pi-\pi$ stacking interaction between the Phe58 benzene ring and the Arg62 guanidyl group (average spacing = 3.6 Å and dihedral angle = 35°). This stacking structure is stabilized by bifurcated Arg62 NεH/NηH···O Phe58 hydrogen bonds (2.93 and 2.92 Å), thus contributing to the stabilization of the α-helical structure. In the case of 4E-BP1, the Cys62 SH group undergoes a S–H···π interaction with the Phe58 benzene ring, although the extent of this interaction is rather limited because of the deviation in the Cys62 SH position from the center of the benzene ring. Another difference is in the orientation of the C-terminal backbone chain. In the conformation of 4E-BP2, the *trans*-oriented Arg63 side chain with respect to Arg62 directs the orientation of the

Journal of PeptideScience

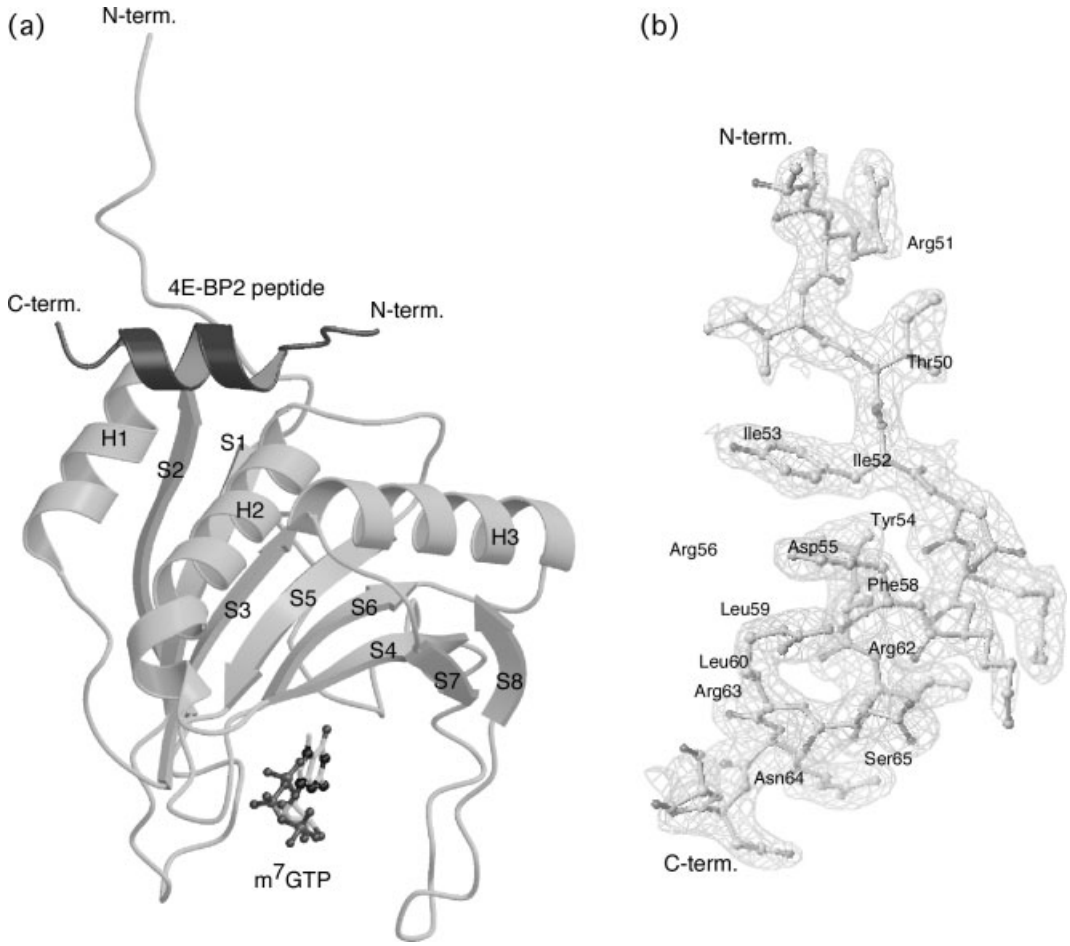

Figure 2. Overall structure of ternary complex of m^{7}GTP–eIF4E–4E-BP2 peptide and 2Fo-Fc omit map of 4E-BP2 peptide. eIF4E (gray) and the 4E-BP2 peptide [Pro47-Ser65] (black) are shown using the ribbon model, and m^{7}GTP is depicted using the stick–bond model. Three α-helices and eight sheets of eIF4E are labeled by H1–H3 and S1–S8, respectively, and the N-terminal moiety of eIF4E is shown by the N-term. The contour of electron density is depicted at the 3σ level.

Asn63-Ser64 sequence toward the direction opposite to 4E-BP1. Consequently, the Ser65 of 4E-BP2 does not participate in the hydrogen bonding with the Asn77 Nδ2H of eIF4E (to be discussed later); however, such a hydrogen bond is formed for 4E-BP1.

The molecular conformation of 4E-BP3 is not yet available. However, the conformation of its eIF4E binding sequence would be similar to that of 4E-BP1, because the influence of the Glu47-Cys48-Lys49 sequence on the conformation of 4E-BP3 could be nearly the same as that of the Glu61-Cys62-Arg63 sequence of 4E-BP1, rather than the Asp62-Arg63-Arg64 sequence of 4E-BP2.

4E-BP Isoform-specific Binding with eIF4E

The binding mode between 4E-BP2 peptide and eIF4E is shown in Figure 4(a) and the difference in the binding mode between 4E-BP1 and 4E-BP2 is shown in Figure 4(b). Hydrogen bonds and selected electrostatic short contacts between both molecules are given in Table 3. Concerning the eIF4E residues associated with the 4E-BP binding selectivity or specificity, Leu39, Trp73, Val69, and Gly139 residues are identified in spectroscopic studies [15]. It is evident from Table 3 that Trp73 and Gly139 participate in the interaction of both 4E-BPs. Furthermore, in the case of 4E-BP2, the planar propyl side chain of Arg63 is stacked on the Trp73 indole ring through hydrophobic interaction (average spacing = 4.0 Å);

Table 2. Comparison of some intramolecular hydrogen bonds and electrostatic short contacts of 4E-BP1 and 4E-BP2 characterizing the conformational features

		Distance (Å)	
Donor	Acceptor	4E-BP1	4E-BP2
Lys57NH	Oδ Asp55	3.11	2.62
Phe58NH	Oδ Asp55	2.87	2.72
Phe58NH	O Asp55	3.33	2.90
Leu59NH	O Asp55	3.24	3.26
Met60NH	O Arg56	2.94	
Leu60NH	O Arg56		2.84
Glu61NH	O Lys57	2.56	
Glu61NH	O Phe58	3.00	
Asp61NH	O Lys57		2.94
Cys62NH	O Phe58	2.81	
Arg62NεH	O Phe58		2.93
Arg62NηH	O Phe58		2.92
Arg62NH	O Leu59		3.26
Arg63NH	O Met60	2.65	
Arg63NH	O Glu61	2.41	
Arg63NH	O Leu60		3.19

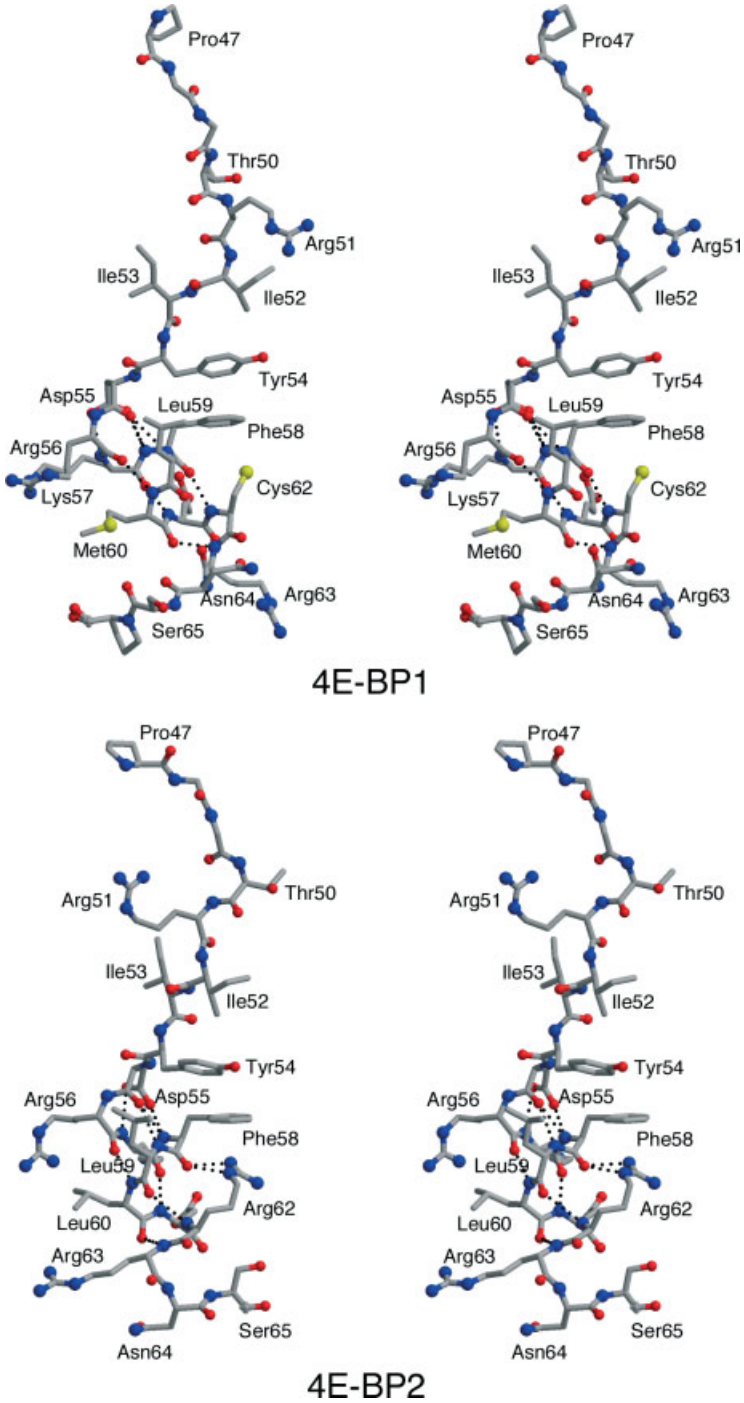

Figure 3. Molecular conformations (in stereo) of 4E-BP1 and 4E-BP2. Dotted lines represent intramolecular hydrogen bonds. Each amino acid residue is shown with a three-code label. The red and blue circles represent oxygen and nitrogen atoms, respectively. Dotted lines represent intramolecular hydrogen bonds reflecting the difference between both molecules.

such an interaction is not induced for 4E-BP1 (Figure 5(a)). This is probably due to the *trans* orientation of the Arg63 side chain with respect to the Arg62 for 4E-BP2, and such conformational constraint is not imposed for the Arg63 residue of 4E-BP1 because of the Cys62 residue (Figure 3). On the other hand, the Leu39 and Val69 residues of eIF4E constitute a compact hydrophobic core in collaboration with the Tyr54, Phe58 and Leu59 residues of 4E-BP2. However, a similar hydrophobic core is also formed by interaction with 4E-BP1. Thus, the binding of Leu39 and Val69 residues of eIF4E appear not to be strong enough to account for the binding selectivity of 4E-BP isoforms (Figure 4).

On the other hand, it is reasonable to consider that the difference in eIF4E binding specificity between 4E-BP1 and 4E-BP2 results mainly from the difference in their 60–62 sequences, i.e. Met-Glu-Cys for 4E-BP1 and Leu-Asp-Arg for 4E-BP2. Ptushkina *et al*. [15] reported that this sequential difference between 4E-BP1 and 4E-BP2 affects the hydrophobic interaction of Met60/Leu60 with the Trp73 indole ring (eIF4E) and the electrostatic interaction of

Journal of PeptideScience

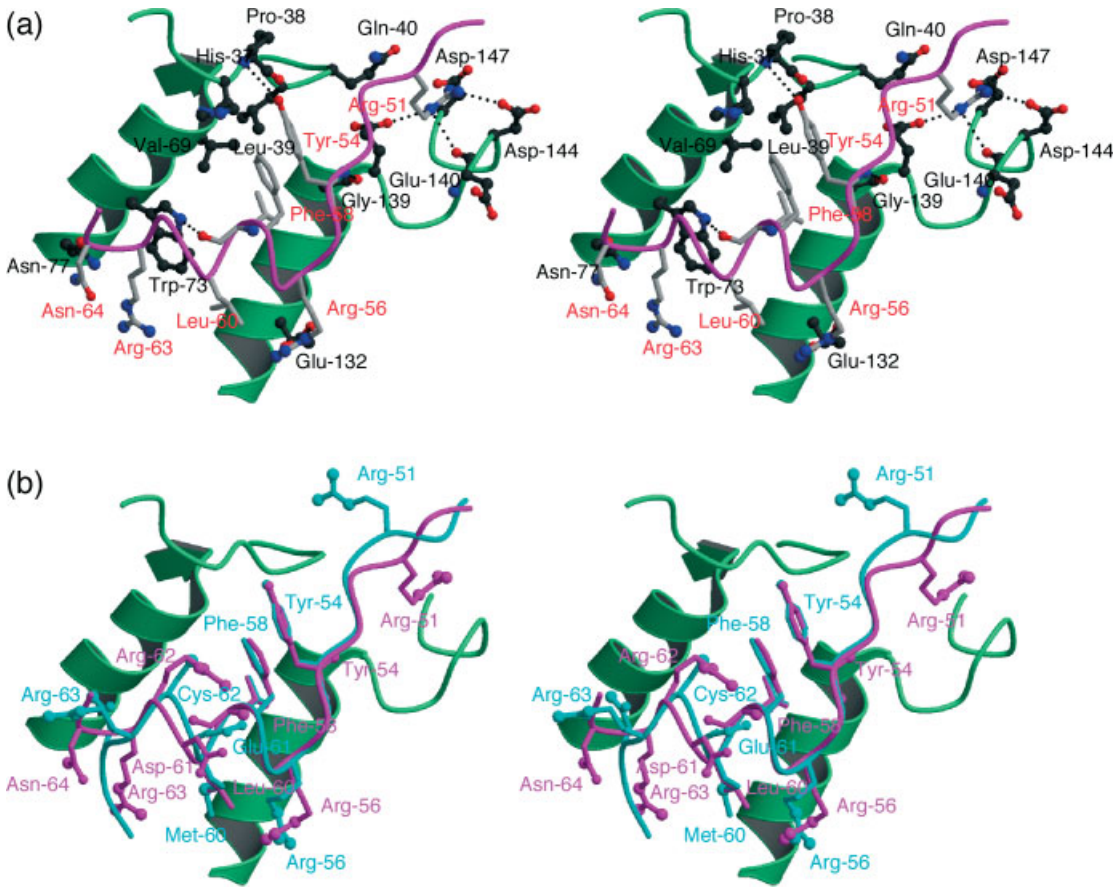

Figure 4. (a) Binding mode (in stereo) of 4E-BP2 peptide (magenta wire) at 4E-BP binding pocket of eIF4E (green) and (b) its superimposition with 4E-BP1 (cyan wire). The N-terminal extended (His37-Gln40, wire), and H1 (Trp73-Asn77) and H2 (Glu132-Gly139) helical (ribbons) regions of eIF4E form the 4E-BP binding pocket. Dotted lines in (a) represent hydrogen bonds between eIF4E and 4E-BP2 peptide.

Table 3. Hydrogen bonds and selected C–H/C═O···π interactions between eIF4E and 4E-BP1/4E-BP2 peptides

4E-BP	Structure[a]	eIF4E	Binding region[b]	Distance(Å)	Interaction type
4E-BP1					
Arg51 NεH	Extend	Gln40 Oε1	N-term	2.67	H-bond
Arg51 Nη2H	Extend	Gln40 O	N-term	2.89	H-bond
Tyr54 NH	Extend	Gly139 O	H2	2.97	H-bond
Tyr54 OηH	Extend	Pro38 O	N-term	2.53	H-bond
Arg56 NεH	Helix	Glu132 Oε1	H2	2.81	H-bond
Phe58 benzene	Helix	His37 imidazole	N-term	~3.7 to 4.0	C–H···π[c]
Leu59 O	Helix	Trp73 Nε1H	H1	2.90	H-bond
Arg63 O	Extend	Trp73 indole	H1	~3.2	C═O π[c]
Asn64 Nδ2H	Extend	Asn77 Oδ1	H1	3.19	H-bond
Ser65 Oγ H	Extend	Asn77 Nδ2	H1	2.53	H-bond
4E-BP2					
Arg51 NεH	Extend	Asp143 O	H2	3.39	H-bond
Arg51 Nη1H	Extend	Asp144 Oδ1	H2	3.04	H-bond
Ile52 NH	Extend	Gln40 Oε1	N-term	2.76	H-bond
Tyr54 NH	Extend	Gly139 O	H2	3.00	H-bond
Arg56 NεH	Helix	Glu132 Oε2	H2	2.93	H-bond
Arg56 NηH	Helix	Glu132 Oε2	H2	2.81	H-bond
Phe58 benzene	Helix	His37 imidazole	N-term	~3.7 to 4.0	C–H π[c]
Leu59 O	Helix	Trp73 Nε1 H	H1	2.85	H-bond

[a] Extend and helix represent the distorted extend and α-helical structure moieties of the 4E-BP peptide, respectively.
[b] N-term, H1 and H2 denote the N-terminal, H1 and H2 helix regions of the eIF4E molecule shown in Figure 3, respectively.
[c] These interactions are of edge-to-face type.

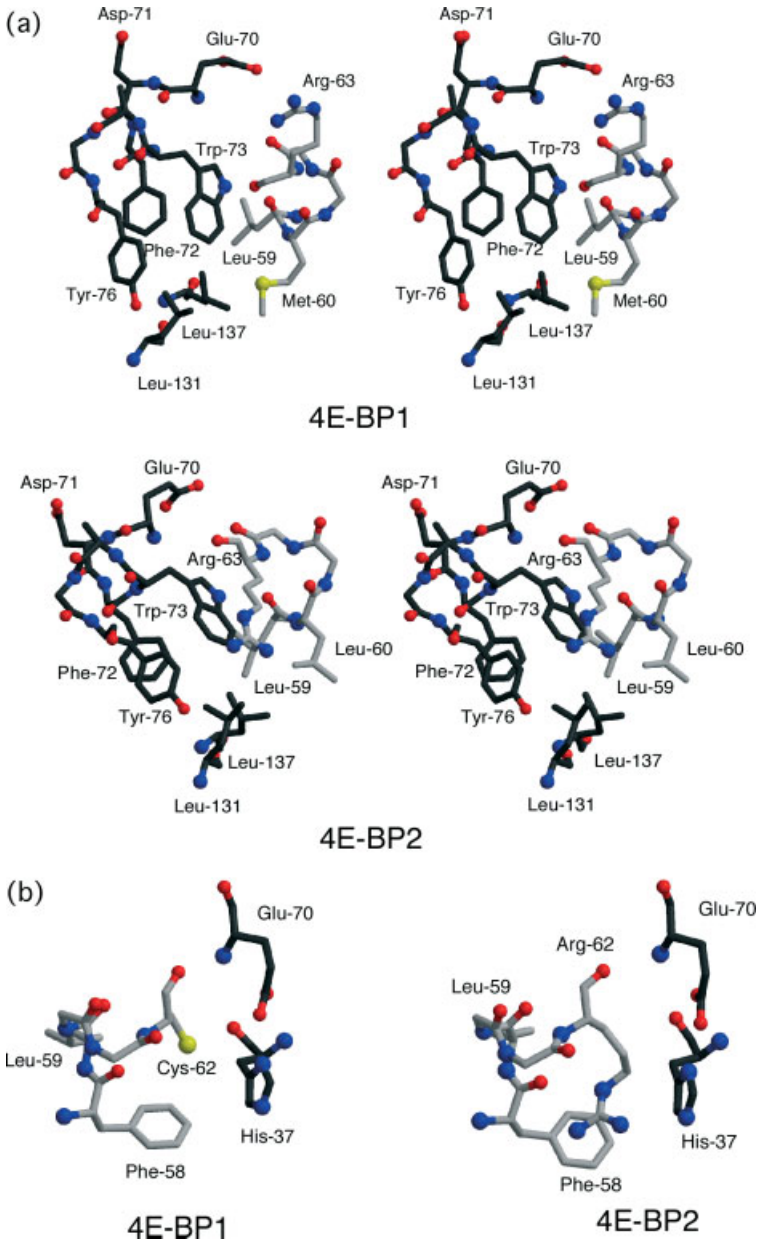

Figure 5. Different interaction mode between 4E-BP1 and 4E-BP2 (gray bond) with eIF4E (dark bond): (a) Leu59/Met60-Trp73 and Leu59/Leu60-Trp73 (in stereo) and (b) Cys62/Phe58-His37/Glu70 and Arg62/Phe58-His37/Glu70.

Cys62/Arg62 with the His37 imidazole ring and Glu70 carboxyl group of eIF4E. To confirm the structural differences between these regions, the crystal structures of the respective complexes were compared in detail. It was clarified that (i) the Trp73 indole ring of eIF4E is significantly affected by the Arg63 side chain of 4E-BP2 through hydrophobic interaction, and this is in contrast to that in the case of 4E-BP1, where the interaction of Trp73 with the Met60 of 4E-BP1 is negligible (Figure 5(a)), and (ii) the guanidyl group of Arg62 orients itself so as to interact with the Phe58 benzene ring of 4E-BP2 and localizes apart from the site of interaction with the His37 imidazole ring and Glu70 carboxyl group of eIF4E (Arg62 NεH$\cdots$His37 Nε 2 and Glu70 Oε = 3.35 and 2.98 Å, respectively), whereas the Cys62 of 4E-BP1 localizes in the range within electrostatic interaction with these residues (Figure 5(b)). Thus, the notable interactions of the Arg62 side chain with the Trp73 indole ring (eIF4E) for 4E-BP2 and of the Cys62 SH group with the His37/Glu70 side chains for 4E-BP1 could be a structural scaffold for differentiating the eIF4E-binding specificity between 4E-BP1 and 4E-BP2. Another notable difference could be observed between the Met60 of 4E-BP1 and the Leu60 of 4E-BP2. The Leu59-Leu60 sequence of 4E-BP2, together with the Leu131 and Leu137 of eIF4E, provides a more compact hydrophobic space around the Trp73 indole ring than the Lue59-Met60 of 4E-BP1 (Figure 5(a)); this could induce the quenching effect of Trp fluorescence intensity more efficiently for the interaction with 4E-BP2 than that with 4E-BP1.

Different Binding Orientation of 4E-BP Terminal Sequence

A difference in binding with eIF4E was also observed between the C-terminal sequences of 4E-BP1 and 4E-BP2 peptides. The Asn64

Journal of PeptideScience

Nδ2H and Ser65 O of 4E-BP1 form hydrogen bonds with Asn77 Oδ1 and Nδ2H of eIF4E, thus directing the C-terminal sequence toward the C-terminal side of eIF4E. In contrast, the *trans*-oriented Arg63 side chain of 4E-BP2 with respect to the Arg62 side chain (Figure 3), which results from the interaction between the Arg62 guanidyl group of 4E-BP2 and the Phe58 benzene ring of eIF4E, directs the orientation of the Asn64-Ser65 sequence toward the opposite side from the case of 4E-BP1, thus turning the sequence toward the N-terminal side of eIF4E.

Conclusion

This work was performed to clarify the structural basis of the difference in eIF4E binding specificity between 4E-BP1 and 4E-BP2. The X-ray crystal structure of the m^{7}GTP–eIF4E–4E-BP2 peptide ternary complex clarified the molecular conformation of the 4E-BP2 peptide and its interaction mode with eIF4E, which was located at the root of the handle of the temple-bell-shaped eIF4E through hydrophilic and hydrophobic interactions. The comparison with the previously determined X-ray result of the m^{7}GpppA–eIF4E–4E-BP1 peptide complex afforded the structural scaffold for the eIF4E binding preference for 4E-BP2 over 4E-BP1, i.e. (i) the stacking of the Arg63 planar side chain on the Trp73 indole ring of eIF4E and (ii) the construction of a compact hydrophobic space around the Trp73 indole ring using the Leu59-Leu60 sequence of 4E-BP2, together with the Leu131 and Leu135 of eIF4E. These structural features explain the eIF4E binding preference for 4E-BP2 over 4E-BP1, determined by the quenching titration of Trp fluorescence, because the masking of the Trp73 indole ring by the hydrophobic groups leads to a large quenching of fluorescence intensity.

References

1 Sonenberg N, Dever TE. Eukaryotic translation initiation factors and regulators. *Curr. Opin. Struct. Biol.* 2003; **13**: 56–63.
2 Sonenberg N, Hinnebusch AG. Regulation of translation initiation in eukaryotes: mechanisms and biological targets. *Cell* 2009; **136**: 731–745.
3 Pause A, Belsham GJ, Gingras AC, Donze O, Lin AA, Laurence JC Jr, Sonenberg N. Insulin-dependent stimulation of protein synthesis by phosphorylation of a regulator of 5′-cap function. *Nature* 1994; **371**: 762–767.
4 Sonenberg N, Gingras AC. The mRNA 5′-cap binding protein eIF4E and control of cell growth. *Curr. Opin. Cell Biol.* 1998; **10**: 268–275.
5 Mader S, Lee H, Pause A, Sonenberg N. The translation initiation factor eIF4E binds to a common motif shared by the translation factor eIF4-γ and the translational repressor 4E-binding proteins. *Mol. Cell. Biol.* 1997; **17**: 6940–6947.
6 Altmann M, Schmitz N, Berset N, Trachsel H. A novel inhibitor of cap-dependent translation initiation in yeast–p20 competes with eIF4G for binding to eIF4E. *EMBO J.* 1997; **16**: 1114–1121.
7 Gingras AC, Gygi SP, Raught B, Polakiewicz RD, Abraham RT, Hoekstra MF, Aebersold R, Sonenberg N. Regulation of 4E-BP1 phosphorylation: a novel two-step mechanism. *Genes Dev.* 1999; **13**: 1422–1437.
8 Tomoo K, Matsushita Y, Fujisaki H, Abiko F, Shen X, Taniguchi T, Miyagawa H, Kitamura K, Miura K, Ishida T. Structural basis for mRNA cap-binding regulation of eukaryotic initiation factor 4E by 4E-binding protein, studied by spectroscopic, X-ray crystal structural, and molecular dynamics simulation methods. *Biochim. Biophys. Acta* 2005; **1753**: 191–208.
9 Marcotrigiano J, Gingras AC, Sonenberg N, Burley, SK. Cap-dependent translation initiation in *Eukaryotes* is regulated by a molecular mimic of eIF4G. *Mol. Cell* 1999; **3**: 707–716.
10 Morino S, Hazama H, Ozaki M, Teraoka Y, Shibata S, Doi M, Ueda H, Ishida T, Uesugi S. Analysis of the mRNA cap-binding ability of human eukaryotic initiation factor-4E by use of recombinant wild-type and mutant forms. *Eur. J. Biochem.* 1996; **239**: 597–601.
11 Pflugrath JW. The finer things in X-ray diffraction data collection. *Acta Crystal.* 1999; **D55**: 1718–1725.
12 Brunger AT, Adams PD, Clore GM, DeLano WL, Gros P, Grosse-Kunstleve RW, Jiang JS, Kuszewski J, Nilges M, Pannu NS, Read RJ, Rice LM, Simonson T, Warren GL. Crystallography & NMR system: A new software suite for macromolecular structure determination. *Acta Crystal.* 1998; **D54**: 905–921.
13 Jones TA. A graphics model building and refinement system for macromolecules. *J. Appl. Cryst.* 1987; **15**: 23–31.
14 Tomoo K, Shen X, Okabe K, Nozoe Y, Fukuhara S, Morino S, Sasaki M, Taniguchi T, Miyagawa H, Kitamura K, Miura K, Ishida T. Structural features of human initiation factor 4E, studied by X-ray crystal analyses and molecular dynamics simulations. *J. Mol. Biol.* 2003; **328**: 365–383.
15 Ptushkina M, von der Haar T, Karim MM, Hughes JMX, McCarthy JE. Repressor binding to a dorsal regulatory site traps human eIF4E in a high cap-affinity state. *EMBO J.* 1999; **18**: 4068–4075.

